PROCEEDINGS OF THE ROYAL SOCIETY A MATHEMATICAL, PHYSICAL & ENGINEERING SCIENCES

Campbell diagrams of weakly anisotropic flexible rotors

O. N. Kirillov

Proc. R. Soc. A 2009 **465**, 2703-2723 first published online 24 June 2009
doi: 10.1098/rspa.2009.0055

PROCEEDINGS OF THE ROYAL SOCIETY A

Proc. R. Soc. A (2009) **465**, 2703–2723
doi:10.1098/rspa.2009.0055
Published online 24 June 2009

Campbell diagrams of weakly anisotropic flexible rotors

By O. N. Kirillov*

Dynamics and Vibrations Group, Department of Mechanical Engineering, Technical University of Darmstadt, Hochschulstraße 1, 64289 Darmstadt, Germany

We consider an axi-symmetric flexible rotor perturbed by dissipative, conservative and non-conservative positional forces originated at the contact with the anisotropic stator. The Campbell diagram of the unperturbed system is a mesh-like structure in the frequency–speed plane with double eigenfrequencies at the nodes. The diagram is convenient for the analysis of the travelling waves in the rotating elastic continuum. Computing sensitivities of the doublets, we find that at every particular node the unfolding of the mesh into the branches of complex eigenvalues in the first approximation is generically determined by only four 2×2 sub-blocks of the perturbing matrix. Selection of the unstable modes that cause self-excited vibrations in the subcritical speed range is governed by the exceptional points at the corners of the singular eigenvalue surfaces—'double coffee filter' and 'viaduct'—which are sharply associated with the crossings of the unperturbed Campbell diagram with the definite symplectic (Krein) signature. The singularities connect the problems of wave propagation in the rotating continua with that of electromagnetic and acoustic wave propagation in non-rotating anisotropic chiral media. As mechanical examples a model of a rotating shaft with two degrees of freedom and a continuous model of a rotating circular string passing through the eyelet are studied in detail.

Keywords: Campbell diagram; flexible rotor; dissipation-induced instabilities; subcritical flutter; symplectic (Krein) signature; non-Hermitian degeneracies

1. Introduction

Bending waves propagate in the circumferential direction of an elastic body of revolution rotating about its axis of symmetry (Bryan 1890; Southwell 1921; Srinivasan & Lauterbach 1971; Ouyang & Mottershead 2001; Genta 2007). The frequencies of the waves plotted against the rotational speed are referred to as the *Campbell diagram* (Campbell 1924; Genta 2007). The spectrum of a perfect rotationally symmetric rotor at standstill has infinitely many double semisimple eigenvalues—the *doublet modes*. Indeed, for $\mathbb{R}^{2\times 2} \ni \mathbf{A} = \mathrm{diag}(\omega_1^2, \omega_2^2)$ and $\mathbf{R} = \begin{pmatrix} \cos\theta & \sin\theta \\ -\sin\theta & \cos\theta \end{pmatrix}$ the restriction $\mathbf{R}^{\mathrm{T}}\mathbf{A}\mathbf{R} = \mathbf{A}$ imposed by equivariance

*kirillov@dyn.tu-darmstadt.de

Received 31 January 2009
Accepted 21 May 2009

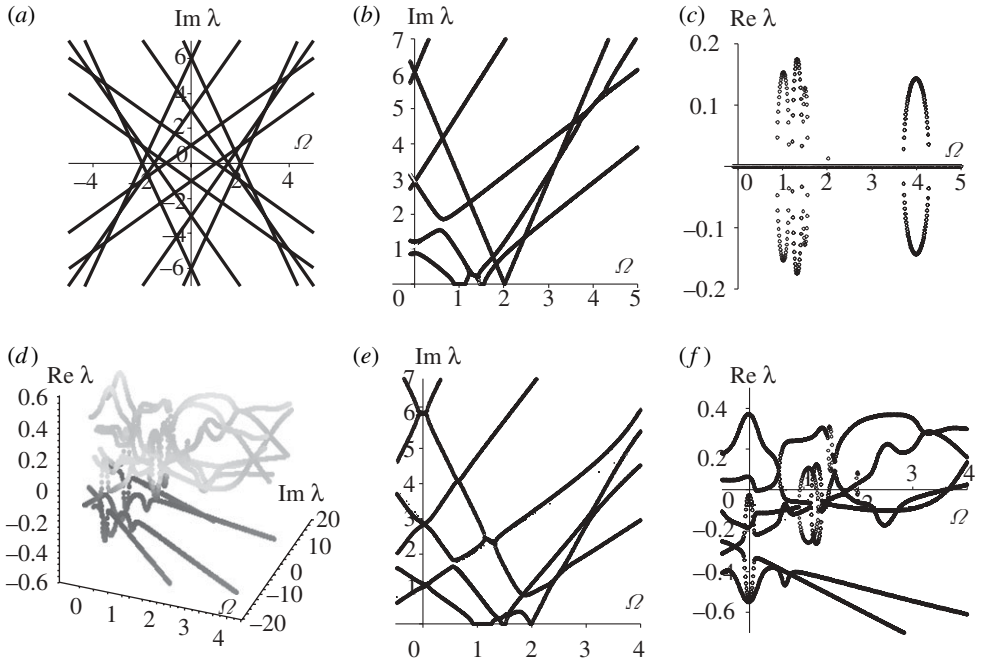

Figure 1. (*a*) The Campbell diagram of the unperturbed system (2.2) with six degrees of freedom (d.f.) in case of $\omega_1 = 1$, $\omega_2 = 3$ and $\omega_3 = 6$; (*b*) the Campbell diagram; (*c*) decay rate plots for the stiffness modification $\kappa \mathbf{K}_1$ with $\kappa = 0.2$; (*d*) unfolding the Campbell diagram owing to perturbation with the matrices $\mathbf{K} = \mathbf{K}_1$, $\mathbf{D} = \mathbf{D}_1$, $\mathbf{N} = \mathbf{N}_1$ and $\kappa = 0.2$, $\delta = 0.1$ and $\nu = 0.2$; (*e*) the corresponding Campbell diagram; and (*f*) decay rate plots.

of the equations of motion with respect to the action of the circle group implies $\omega_1^2 = \omega_2^2$ (Dellnitz *et al.* 1992; Nagata & Namachchivaya 1998). By this reason, the Campbell diagram contains the eigenvalue branches originated after splitting of the doublets by gyroscopic forces (Bryan 1890). The branches correspond to simple pure imaginary eigenvalues and intersect each other forming a *spectral mesh* (Günther & Kirillov 2006) in the frequency–speed plane with the doublets at the nodes (figure 1*a*). Perturbations of the axially symmetric rotor by dissipative, conservative and non-conservative positional forces, caused by its contact with the anisotropic stator, generically unfold the spectral mesh of pure imaginary eigenvalues of the Campbell diagram into separate branches of complex eigenvalues in the $(\Omega, \mathrm{Im}\,\lambda, \mathrm{Re}\,\lambda)$-space (figure 1*d*). Nevertheless, the eigenvalue branches in the perturbed Campbell diagram can both avoid crossings and cross each other (figure 1*e*). Moreover, the real parts of the perturbed eigenvalues plotted against the rotational speed—*decay rate plots* (Genta 2007)—can also intersect each other and inflate into 'bubbles' (figure 1*f*). This complicated behaviour is difficult to predict and even to interpret according to the studies of numerous mechanical systems (Ono *et al.* 1991; Chen & Bogy 1992; Mottershead & Chan 1995; Yang & Hutton 1995; Tian & Hutton 1999; Xiong *et al.* 2002; Canchi & Parker 2006; Young & Lin 2006; Genta 2007; Lesaffre *et al.* 2007; Spelsberg-Korspeter *et al.* 2009). The present work reveals

that the unfolding of the Campbell diagrams is determined by a limited number of local scenarios for eigenvalues as a function of parameters, which form stratified manifolds.

2. A model of a weakly anisotropic rotor system

In general, the imperfections in the rotor and stator complicate the linearized equations of motion, making them non-self-adjoint with time-dependent coefficients. Nevertheless, an axially symmetric rotor with an anisotropic stator as well as an asymmetric rotor with an isotropic stator are autonomous non-conservative gyroscopic systems (Genta 2007). Neglecting the centrifugal stiffness without loss of generality, we consider the finite-dimensional anisotropic rotor system

$$\ddot{\mathbf{x}} + (2\Omega\mathbf{G} + \delta\mathbf{D})\dot{\mathbf{x}} + (\mathbf{P} + \Omega^2\mathbf{G}^2 + \kappa\mathbf{K} + \nu\mathbf{N})\mathbf{x} = 0, \tag{2.1}$$

which is a perturbation of the isotropic one (Nagata & Namachchivaya 1998)

$$\ddot{\mathbf{x}} + 2\Omega\mathbf{G}\dot{\mathbf{x}} + (\mathbf{P} + \Omega^2\mathbf{G}^2)\mathbf{x} = 0, \tag{2.2}$$

where $\mathbf{x} = \mathbb{R}^{2n}$, $\mathbf{P} = \mathrm{diag}(\omega_1^2, \omega_1^2, \omega_2^2, \omega_2^2, \ldots, \omega_n^2, \omega_n^2)$ is the stiffness matrix and $\mathbf{G} = -\mathbf{G}^{\mathrm{T}}$ is the matrix of gyroscopic forces defined as

$$\mathbf{G} = \mathrm{blockdiag}(\mathbf{J}, 2\mathbf{J}, \ldots, n\mathbf{J}) \quad \text{and} \quad \mathbf{J} = \begin{pmatrix} 0 & -1 \\ 1 & 0 \end{pmatrix}. \tag{2.3}$$

The matrices of non-Hamiltonian perturbation corresponding to velocity-dependent dissipative forces, $\mathbf{D} = \mathbf{D}^{\mathrm{T}}$, and non-conservative positional forces, $\mathbf{N} = -\mathbf{N}^{\mathrm{T}}$, as well as the matrix $\mathbf{K} = \mathbf{K}^{\mathrm{T}}$ of the Hamiltonian perturbation that breaks the rotational symmetry, can depend on the rotational speed Ω. The intensity of the perturbation is controlled by the parameters δ, κ and ν. Putting $\kappa = 0$ and $\nu = 0$ in equation (2.1) yields the model considered in Nagata & Namachchivaya (1998).

At $\Omega = 0$, the eigenvalues $\pm i\omega_s$, $\omega_s > 0$, of the isotropic rotor equation (2.2) are double semisimple with two linearly independent eigenvectors. The sequence of the frequencies ω_s, where s is an integer index, is usually different for various bodies of revolution. For example, $\omega_s = s$ corresponds to the natural frequency $f_s = s/2\pi r\sqrt{P/\rho}$ of a circular string of radius r, circumferential tension P and mass density ρ per unit length (Yang & Hutton 1995).

Substituting $\mathbf{x} = \mathbf{u}\exp(\lambda t)$ into equation (2.2), we arrive at the eigenvalue problem

$$\mathbf{L}_0(\Omega)\mathbf{u} := (\mathbf{I}\lambda^2 + 2\Omega\mathbf{G}\lambda + \mathbf{P} + \Omega^2\mathbf{G}^2)\mathbf{u} = 0. \tag{2.4}$$

The eigenvalues of the operator $\mathbf{L}_0$ are found in the explicit form

$$\lambda_s^+ = i\omega_s + is\Omega, \quad \overline{\lambda_s^-} = -i\omega_s + is\Omega, \quad \lambda_s^- = i\omega_s - is\Omega \quad \text{and} \quad \overline{\lambda_s^+} = -i\omega_s - is\Omega, \tag{2.5}$$

where the overbar denotes complex conjugate. The eigenvectors of λ_s^+ and $\overline{\lambda_s^-}$ are

$$\boldsymbol{u}_1^+ = (-i, 1, 0, 0, \ldots, 0, 0)^{\mathrm{T}}, \ldots, \ \boldsymbol{u}_n^+ = (0, 0, \ldots, 0, 0, -i, 1)^{\mathrm{T}}, \tag{2.6}$$

where the imaginary unit holds the $(2s-1)$st position in the vector $\boldsymbol{u}_s^+$. The eigenvectors, corresponding to the eigenvalues λ_s^- and $\overline{\lambda_s^+}$, are simply $\boldsymbol{u}_s^- = \overline{\boldsymbol{u}_s^+}$.

For $\Omega > 0$, simple eigenvalues λ_s^+ and λ_s^- correspond to the forward and backward travelling waves, respectively, that propagate in the circumferential direction of the rotor. At the angular velocity $\Omega_s^{\mathrm{cr}} = \omega_s/s$ the frequency of the sth backward travelling wave vanishes to zero, so that the wave remains stationary in the non-rotating frame. We assume further in the text that the sequence of the doublets $i\omega_s$ has the property $\omega_{s+1} - \omega_s \geq \Omega_s^{\mathrm{cr}}$, which implies the existence of the minimal *critical* speed $\Omega_{\mathrm{cr}} = \Omega_1^{\mathrm{cr}} = \omega_1$. When the speed of rotation exceeds the critical speed, some backward waves, corresponding to the eigenvalues $\overline{\lambda_s^-}$, travel slower than the disc rotation speed and appear to be travelling forward (reflected waves).

In figure 1*a*, the spectral mesh (2.5) is shown for the six d.f. system (2.2) with the frequencies $\omega_1 = 1$, $\omega_2 = 3$ and $\omega_3 = 6$ that imitate the distribution of the doublets of a circular ring (Canchi & Parker 2006). To illustrate typical unfolding of the Campbell diagram, we plot in figure 1*d–f* the eigenvalues of the six d.f. system (2.1) with $\kappa = 0.2$, $\delta = 0.1$, $\nu = 0.2$, $\omega_1 = 1$, $\omega_2 = 3$ and $\omega_3 = 6$ for the specific symmetry-breaking matrix $\mathbf{K} = \mathbf{K}_1$, $(\mathbf{K}_1 = \mathbf{K}_1^{\mathrm{T}})$, whose non-zero entries are $k_{11} = 1$, $k_{12} = 2$, $k_{13} = 1$, $k_{14} = 2$, $k_{22} = 1$, $k_{23} = 3$, $k_{24} = 4$, $k_{33} = -3$, $k_{44} = -2.5$, $k_{55} = 4$ and $k_{66} = 2$, and for the matrices $\mathbf{D} = \mathbf{D_1}$ and $\mathbf{N} = \mathbf{N}_1$, where

$$\mathbf{D}_1 = \begin{pmatrix} -1 & 2 & 1 & 7 & 2 & -2 \\ 2 & 3 & -2 & -4 & 3 & 1 \\ 1 & -2 & 1 & 8 & 2 & 1 \\ 7 & -4 & 8 & 3 & -2 & 3 \\ 2 & 3 & 2 & -2 & 5 & 5 \\ -2 & 1 & 1 & 3 & 5 & 6 \end{pmatrix} \quad \text{and} \quad \mathbf{N}_1 = \begin{pmatrix} 0 & -1 & 1 & -1 & -3 & 8 \\ 1 & 0 & 2 & 3 & 2 & 4 \\ -1 & -2 & 0 & 7 & 1 & 3 \\ 1 & -3 & -7 & 0 & 8 & 2 \\ 3 & -2 & -1 & -8 & 0 & 2 \\ -8 & -4 & -3 & -2 & -2 & 0 \end{pmatrix}.$$

In the following, we classify and interpret the typical behaviour of the eigenvalues of weakly anisotropic rotor system (2.1) with the use of the perturbation formula for the doublets of the spectral mesh (2.5), which we derive in the next section.

3. Perturbation of the doublets

Introducing the indices $\alpha, \beta, \varepsilon, \sigma = \pm 1$, we find that the eigenvalue branches $\lambda_s^\varepsilon = i\alpha\omega_s + i\varepsilon s\Omega$ and $\lambda_t^\sigma = i\beta\omega_t + i\sigma t\Omega$ cross each other at $\Omega = \Omega_0$ with the origination of the double eigenvalue $\lambda_0 = i\omega_0$ with two linearly independent eigenvectors $\boldsymbol{u}_s^\varepsilon$ and $\boldsymbol{u}_t^\sigma$, where

$$\Omega_0 = \frac{\alpha\omega_s - \beta\omega_t}{\sigma t - \varepsilon s} \quad \text{and} \quad \omega_0 = \frac{\alpha\sigma\omega_s t - \beta\varepsilon\omega_t s}{\sigma t - \varepsilon s}. \tag{3.1}$$

Let $\mathbf{M}$ be one of the matrices $\mathbf{D}$, $\mathbf{K}$ or $\mathbf{N}$. In the following, we decompose the matrix $\mathbf{M}\in\mathbb{R}^{2n\times 2n}$ into n^2 blocks $\mathbf{M}_{st}\in\mathbb{R}^{2\times 2}$, where $s,t=1,2,\ldots,n$

$$\mathbf{M}=\begin{pmatrix} * & * & * & * & * \\ * & \mathbf{M}_{ss} & \cdots & \mathbf{M}_{st} & * \\ * & \vdots & \ddots & \vdots & * \\ * & \mathbf{M}_{ts} & \cdots & \mathbf{M}_{tt} & * \\ * & * & * & * & * \end{pmatrix} \quad\text{and}\quad \mathbf{M}_{st}=\begin{pmatrix} m_{2s-1,2t-1} & m_{2s-1,2t} \\ m_{2s,2t-1} & m_{2s,2t} \end{pmatrix}. \tag{3.2}$$

Note that $\mathbf{D}_{st}=\mathbf{D}_{ts}^{\mathrm{T}}$, $\mathbf{K}_{st}=\mathbf{K}_{ts}^{\mathrm{T}}$ and $\mathbf{N}_{st}=-\mathbf{N}_{ts}^{\mathrm{T}}$.

We consider a general perturbation of the matrix operator of the isotropic rotor $\mathbf{L}_0(\Omega)+\Delta\mathbf{L}(\Omega)$. The size of the perturbation $\Delta\mathbf{L}(\Omega)=\delta\lambda\mathbf{D}+\kappa\mathbf{K}+\nu\mathbf{N}\sim\epsilon$ is small, where $\epsilon=\|\Delta\mathbf{L}(\Omega_0)\|$ is the Frobenius norm of the perturbation at $\Omega=\Omega_0$. For small $\Delta\Omega=|\Omega-\Omega_0|$ and ϵ, the increment to the doublet $\lambda_0=i\omega_0$ with the eigenvectors $\boldsymbol{u}_s^{\varepsilon}$ and $\boldsymbol{u}_t^{\sigma}$ is given by the formula $\det(\mathbf{R}+(\lambda-\lambda_0)\mathbf{Q})=0$ (Kirillov *et al.* 2005; Kirillov 2008), where the entries of the 2×2 matrices $\mathbf{Q}$ and $\mathbf{R}$ are

$$\left.\begin{aligned} Q_{st}^{\varepsilon\sigma} &= 2i\omega_0(\bar{\boldsymbol{u}}_s^{\varepsilon})^{\mathrm{T}}\boldsymbol{u}_t^{\sigma}+2\Omega_0(\bar{\boldsymbol{u}}_s^{\varepsilon})^{\mathrm{T}}\mathbf{G}\boldsymbol{u}_t^{\sigma}, \\ R_{st}^{\varepsilon\sigma} &= (2i\omega_0(\bar{\boldsymbol{u}}_s^{\varepsilon})^{\mathrm{T}}\mathbf{G}\boldsymbol{u}_t^{\sigma}+2\Omega_0(\bar{\boldsymbol{u}}_s^{\varepsilon})^{\mathrm{T}}\mathbf{G}^2\boldsymbol{u}_t^{\sigma})(\Omega-\Omega_0) \\ &\quad +i\omega_0(\bar{\boldsymbol{u}}_s^{\varepsilon})^{\mathrm{T}}\mathbf{D}\boldsymbol{u}_t^{\sigma}\delta+(\bar{\boldsymbol{u}}_s^{\varepsilon})^{\mathrm{T}}\mathbf{K}\boldsymbol{u}_t^{\sigma}\kappa+(\bar{\boldsymbol{u}}_s^{\varepsilon})^{\mathrm{T}}\mathbf{N}\boldsymbol{u}_t^{\sigma}\nu. \end{aligned}\right\} \tag{3.3}$$

Calculating the coefficients (3.3) with the eigenvectors (2.6), we find the real and imaginary parts of the sensitivity of the doublet $\lambda_0=i\omega_0$ at the crossing (3.1)

$$\left.\begin{aligned} \operatorname{Re}\lambda &= -\frac{1}{8}\left(\frac{\operatorname{Im}A_1}{\alpha\omega_s}+\frac{\operatorname{Im}B_1}{\beta\omega_t}\right)\pm\sqrt{\frac{|c|-\operatorname{Re}c}{2}}, \\ \operatorname{Im}\lambda &= \omega_0+\frac{\Delta\Omega}{2}(s\varepsilon+t\sigma)+\frac{\kappa}{8}\left(\frac{\operatorname{tr}\mathbf{K}_{ss}}{\alpha\omega_s}+\frac{\operatorname{tr}\mathbf{K}_{tt}}{\beta\omega_t}\right)\pm\sqrt{\frac{|c|+\operatorname{Re}c}{2}}, \end{aligned}\right\} \tag{3.4}$$

where $c=\operatorname{Re}c+i\operatorname{Im}c$ with

$$\left.\begin{aligned} \operatorname{Im}c &= \frac{\alpha\omega_t\operatorname{Im}A_1-\beta\omega_s\operatorname{Im}B_1}{8\omega_s\omega_t}(s\varepsilon-t\sigma)\Delta\Omega \\ &\quad +\kappa\frac{(\alpha\omega_s\operatorname{tr}\mathbf{K}_{tt}-\beta\omega_t\operatorname{tr}\mathbf{K}_{ss})(\alpha\omega_s\operatorname{Im}B_1-\beta\omega_t\operatorname{Im}A_1)}{32\omega_s^2\omega_t^2} \\ &\quad -\alpha\beta\kappa\frac{\operatorname{Re}A_2\operatorname{tr}\mathbf{K}_{st}\mathbf{J}_{\varepsilon\sigma}-\operatorname{Re}B_2\operatorname{tr}\mathbf{K}_{st}\mathbf{I}_{\varepsilon\sigma}}{8\omega_s\omega_t}, \\ \operatorname{Re}c &= \left(\frac{t\sigma-s\epsilon}{2}\Delta\Omega+\kappa\frac{\beta\omega_s\operatorname{tr}\mathbf{K}_{tt}-\alpha\omega_t\operatorname{tr}\mathbf{K}_{ss}}{8\omega_s\omega_t}\right)^2 \\ &\quad +\alpha\beta\frac{(\operatorname{tr}\mathbf{K}_{st}\mathbf{J}_{\varepsilon\sigma})^2+(\operatorname{tr}\mathbf{K}_{st}\mathbf{I}_{\varepsilon\sigma})^2}{16\omega_s\omega_t}\kappa^2 \\ &\quad -\frac{(\alpha\omega_s\operatorname{Im}B_1-\beta\omega_t\operatorname{Im}A_1)^2+4\alpha\beta\omega_s\omega_t((\operatorname{Re}A_2)^2+(\operatorname{Re}B_2)^2)}{64\omega_s^2\omega_t^2}. \end{aligned}\right\} \tag{3.5}$$

The coefficients A_1, A_2 and B_1, B_2 depend only on those entries of the matrices $\mathbf{D}$, $\mathbf{K}$ and $\mathbf{N}$ that belong to the four 2×2 blocks (3.2) with the indices s and t

$$\left.\begin{aligned} A_1 &= \delta\lambda_0 \operatorname{tr}\mathbf{D}_{ss}+\kappa \operatorname{tr}\mathbf{K}_{ss}+\varepsilon 2i\nu n_{2s-1,2s},\\ A_2 &= \sigma\nu \operatorname{tr}\mathbf{N}_{st}\mathbf{I}_{\varepsilon\sigma}+i(\delta\lambda_0 \operatorname{tr}\mathbf{D}_{st}\mathbf{J}_{\varepsilon\sigma}+\kappa \operatorname{tr}\mathbf{K}_{st}\mathbf{J}_{\varepsilon\sigma}),\\ B_1 &= \delta\lambda_0 \operatorname{tr}\mathbf{D}_{tt}+\kappa \operatorname{tr}\mathbf{K}_{tt}+\sigma 2i\nu n_{2t-1,2t},\\ B_2 &= \sigma\nu \operatorname{tr}\mathbf{N}_{st}\mathbf{J}_{\varepsilon\sigma}-i(\delta\lambda_0 \operatorname{tr}\mathbf{D}_{st}\mathbf{I}_{\varepsilon\sigma}+\kappa \operatorname{tr}\mathbf{K}_{st}\mathbf{I}_{\varepsilon\sigma}), \end{aligned}\right\} \tag{3.6}$$

where

$$\mathbf{I}_{\varepsilon\sigma}=\begin{pmatrix}\varepsilon & 0\\ 0 & \sigma\end{pmatrix} \quad \text{and} \quad \mathbf{J}_{\varepsilon\sigma}=\begin{pmatrix}0 & -\sigma\\ \varepsilon & 0\end{pmatrix}. \tag{3.7}$$

Therefore, we have identified the elements of the perturbing matrices that control practically important *eigenvalue assignment* (Ouyang 2008; Kirillov 2009*a*,*b*) near every particular node (Ω_0,ω_0) of the spectral mesh.

4. MacKay's eigenvalue cones and instability bubbles

Modification of the stiffness matrix induced by the elastic support interacting with the rotating continua is typical in the models of rotating shafts (Shieh & Masur 1968), computer disk drives (Ono *et al.* 1991; Chen & Bogy 1992), circular saws (Yang & Hutton 1995; Tian & Hutton 1999; Xiong *et al.* 2002), car brakes (Mottershead & Chan 1995; Hervé *et al.* 2008; Spelsberg-Korspeter *et al.* 2009) and turbine wheels (Genta 2007; Lesaffre *et al.* 2007).

Assuming $\delta=0$ and $\nu=0$ in equation (3.4), we find that the eigenvalues of the system (2.5) with the stiffness modification $\kappa\mathbf{K}$ either are pure imaginary ($\operatorname{Re}\lambda=0$) and form a conical surface in the $(\Omega,\kappa,\operatorname{Im}\lambda)$-space with the apex at the point $(\Omega_0,0,\omega_0)$

$$\left(\operatorname{Im}\lambda-\omega_0-\frac{\kappa}{8}\left(\frac{\operatorname{tr}\mathbf{K}_{ss}}{\alpha\omega_s}+\frac{\operatorname{tr}\mathbf{K}_{tt}}{\beta\omega_t}\right)-\frac{\Omega-\Omega_0}{2}(s\varepsilon+t\sigma)\right)^2=\operatorname{Re}c, \tag{4.1}$$

see figure 2*a*, or they are complex and in the $(\Omega,\kappa,\operatorname{Re}\lambda)$-space their real parts originate a cone $(\operatorname{Re}\lambda)^2=-\operatorname{Re}c$ with the apex at the point $(\Omega_0,0,0)$ figure 2*c*. In the $(\Omega,\kappa,\operatorname{Im}\lambda)$-space, the corresponding imaginary parts belong to the plane

$$\operatorname{Im}\lambda=\omega_0+\frac{\kappa}{8}\left(\frac{\operatorname{tr}\mathbf{K}_{ss}}{\alpha\omega_s}+\frac{\operatorname{tr}\mathbf{K}_{tt}}{\beta\omega_t}\right)+\frac{\Omega-\Omega_0}{2}(s\varepsilon+t\sigma), \tag{4.2}$$

which is attached to the cone (4.1) as shown in figure 2*b*.

The existence of eigenvalues with $\operatorname{Re}\lambda\neq 0$ depends on the sign of $\alpha\beta$. It is negative only if the crossing in the Campbell diagram is formed by the eigenvalue branch of the reflected wave and by that of either the forward or backward travelling wave. Otherwise, $\alpha\beta>0$. Owing to the property $\omega_{s+1}-\omega_s\geq\Omega_s^{\mathrm{cr}}$, the crossings of the reflected wave with the forward and backward travelling waves occur only in the *supercritical* speed range $|\Omega|\geq\Omega_{\mathrm{cr}}$. The crossings with $\alpha\beta>0$ are situated in both the super- and *subcritical* ($|\Omega|<\Omega_{\mathrm{cr}}$) ranges. Therefore, the eigenvalues with $\operatorname{Re}\lambda\neq 0$ originate only near the supercritical crossings of the eigenvalue branches λ_s^{ε} and λ_t^{σ} with $\alpha\beta<0$, when the parameters in the

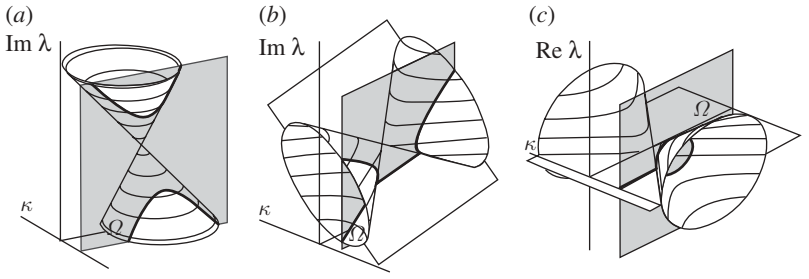

Figure 2. Eigenvalue surfaces (MacKay 1986) and (bold lines) their cross sections in the plane $\kappa = \text{const.}$ (grey): (*a*) a near-vertically oriented cone $\operatorname{Im}\lambda(\Omega,\kappa)$ in the subcritical range ($\operatorname{Re}\lambda = 0$); (*b*) imaginary parts forming a near-horizontally oriented cone (4.1) with the attached membrane (4.2); and (*c*) the real parts forming a near-horizontally oriented cone $(\operatorname{Re}\lambda)^2 = -\operatorname{Re} c$ with the attached membrane $\operatorname{Re}\lambda = 0$ in the supercritical range.

(Ω,κ)-plane are in the sector $\operatorname{Re} c < 0$ bounded by the straight lines $\operatorname{Re} c = 0$

$$\kappa = \frac{4(s\varepsilon - t\sigma)(\Omega - \Omega_0)}{(k_{2t-1,2t-1}+k_{2t,2t})/\beta\omega_t - (k_{2s-1,2s-1}+k_{2s,2s})/\alpha\omega_s \pm 2\sqrt{((\varepsilon k_{2s-1,2t-1} + \sigma k_{2s,2t})^2 + (\varepsilon k_{2s-1,2t} - \sigma k_{2s,2t-1})^2)/ - \alpha\beta\omega_s\omega_t}}. \tag{4.3}$$

As for $\alpha\beta < 0$ the cones of the real parts $(\operatorname{Re}\lambda)^2 = -\operatorname{Re} c$ are near-horizontally oriented and extended along the κ-axis in the $(\Omega,\kappa,\operatorname{Re}\lambda)$-space, their cross-sections by the planes $\kappa = \text{const.}$ are ellipses, as shown in figures 1*c* and 2*c*. As a part of the ellipse corresponds to the eigenvalues with positive real parts, the ellipse is called the *bubble of instability* (MacKay & Saffman 1986). Equation (4.3) is, therefore, a linear approximation to the boundary of the domain of instability, which is divergence (parametric resonance) for $\Omega_0 = \Omega_s^{\mathrm{cr}}$ and flutter (combination resonance) otherwise. The near-horizontal orientation of the corresponding cones of imaginary parts (4.1) in the $(\Omega,\kappa,\operatorname{Im}\lambda)$-space explains deformation in the presence of the perturbation $\kappa\mathbf{K}$ of the crossings with $\alpha\beta < 0$ into the branches of a hyperbola connected by a straight line in the Campbell diagram (figures 1*b* and 2*b*).

Near the crossings with $\alpha\beta > 0$, the perturbed eigenvalues are pure imaginary (stability). The corresponding cones of imaginary parts (4.1) are near-vertically oriented in the $(\Omega,\kappa,\operatorname{Im}\lambda)$-space, figure 2*a*. In the plane $\kappa = \text{const.}$, this yields the *avoided crossing* (MacKay 1986; MacKay & Saffman 1986), which is approximated by a hyperbola shown by the bold lines in figure 2*a* (cf. figure 1*b*).

The conical singularities of the eigenvalue surfaces in the Hamiltonian systems are traced back to the works of Hamilton himself, who predicted the effect of conical refraction of light in birefringent crystals (Hamilton 1833; Berry & Jeffrey 2007). Later on, the conical singularities of eigenvalue surfaces were found in atomic, nuclear and molecular physics (Von Neumann & Wigner 1929; Teller 1937; Mondragon & Hernandez 1993). Nowadays they bear a name of Hamilton's *diabolical points* (Berry & Jeffrey 2007). The existence of the two different orientations of the eigenvalue cones in the Hamiltonian systems was established in MacKay (1986). This result is based on the works of Williamson (1936) and Krein (1983), who introduced the signature of eigenvalues known as the

symplectic signature in the Hamiltonian mechanics (MacKay & Sepulchre 1998) and as the *Krein signature* in a broader context of the theory of Krein spaces (Kirillov *et al.* 2009).

To evaluate the symplectic signatures, we reduce equation (2.2) to $\dot{\mathbf{y}} = \mathbf{A}\mathbf{y}$, where

$$\mathbf{A} = \begin{pmatrix} -\Omega\mathbf{G} & \mathbf{I}_n \\ -\mathbf{P} & -\Omega\mathbf{G} \end{pmatrix} = \mathbf{J}_{2n}\mathbf{A}^{\mathrm{T}}\mathbf{J}_{2n}, \quad \mathbf{J}_{2n} = \begin{pmatrix} 0 & -\mathbf{I}_n \\ \mathbf{I}_n & 0 \end{pmatrix} \quad \text{and} \quad \mathbf{y} = \begin{pmatrix} \mathbf{x} \\ \dot{\mathbf{x}} + \Omega\mathbf{G}\mathbf{x} \end{pmatrix}. \tag{4.4}$$

The Hamiltonian symmetry of the matrix $\mathbf{A}$ implies its self-adjointness in a Krein space with the indefinite inner product $[\mathbf{a}, \mathbf{b}] = \bar{\mathbf{b}}^{\mathrm{T}}\mathbf{J}_{2n}\mathbf{a}$, $\mathbf{a}, \mathbf{b} \in \mathbb{C}^{2n}$. The matrix $\mathbf{A}$ has the eigenvalues $\lambda_s^{\pm}$ given by the formulas (2.5) with the eigenvectors

$$\boldsymbol{a}_s^{++} = \begin{pmatrix} \boldsymbol{u}_s^{+} \\ \lambda_s^{+}\boldsymbol{u}_s^{+} + \Omega\mathbf{G}\boldsymbol{u}_s^{+} \end{pmatrix} \quad \text{and} \quad \boldsymbol{a}_s^{+-} = \begin{pmatrix} \boldsymbol{u}_s^{-} \\ \lambda_s^{-}\boldsymbol{u}_s^{-} + \Omega\mathbf{G}\boldsymbol{u}_s^{-} \end{pmatrix}, \tag{4.5}$$

where the vectors $\boldsymbol{u}_s^{\pm}$ are determined by expressions (2.6). As $i[\boldsymbol{a}_s^{++}, \boldsymbol{a}_s^{++}] = i[\boldsymbol{a}_s^{+-}, \boldsymbol{a}_s^{+-}] = 4\omega_s > 0$, the eigenvalues λ_s^{+} and λ_s^{-} of the forward- and backward travelling waves acquire *positive symplectic* (*Krein*) *signature*. The eigenvalues $\overline{\lambda_s^{+}}$ and $\overline{\lambda_s^{-}}$ of the reflected waves with $i[\boldsymbol{a}_s^{-+}, \boldsymbol{a}_s^{-+}] = i[\boldsymbol{a}_s^{--}, \boldsymbol{a}_s^{--}] = -4\omega_s < 0$, have the opposite, *negative symplectic* (*Krein*) *signature* (MacKay 1986; MacKay & Sepulchre 1998). The signature of an eigenvalue in the Campbell diagram coincides with the sign of the doublet at $\Omega = 0$, from which it is branched, and does not change with the variation of Ω. This implies $\alpha\beta > 0$ and near-vertically oriented cones of imaginary parts (4.1) at the crossings of eigenvalue branches with *definite* (positive) signature and $\alpha\beta < 0$ and near-horizontally oriented cones of imaginary parts (4.1) at the crossings with *mixed* signature (MacKay 1986).

The symplectic signature coincides with the sign of the second derivative of energy, which is a non-degenerate definite quadratic form on the real invariant space associated to a complex conjugate pair of simple pure imaginary non-zero eigenvalues (MacKay 1986). Interaction of waves with positive and negative energy is a well-known mechanism of instability of the moving fluids and plasmas (MacKay 1986; Stepanyants & Fabrikant 1989; Hirota & Fukumoto 2008); in rotor dynamics, this yields flutter in the supercritical speed range, which is known as the mass and stiffness instabilities (Mottershead & Chan 1995; Genta 2007).

Therefore, in the case when anisotropy of the stator is caused by the stiffness modification only, the unfolding of the Campbell diagram is completely described by one-parameter slices of the two-parameter MacKay's eigenvalue cones. As there are only two possible spatial orientations of the cones corresponding to either definite or mixed symplectic signatures, all one has to do to predict the unfolding of the Campbell diagram into avoided crossings or into bubbles of instability is to calculate the signatures of the appropriate eigenvalues of the isotropic rotor. In the following, we develop MacKay's theory further and show that even in the presence of non-Hamiltonian perturbations, all the observed peculiarities of the Campbell diagrams and decay rate plots are one-parameter slices of the eigenvalue surfaces near a limited number of other singularities whose type is dictated by the definiteness of the symplectic signature of the double eigenvalues at the crossings.

5. Double coffee filter singularity near the crossings with definite symplectic (Krein) signature

Understanding general rules of unfolding the Campbell diagrams of weakly anisotropic rotor systems in the presence of dissipative and non-conservative perturbations is important for linear stability analysis and for interpretation of numerical data in both low- and high-speed applications (Genta 2007). In the latter, *supercritical flutter and divergence* instabilities are easily excited near the crossings with the mixed symplectic signature just by the Hamiltonian perturbations like stiffness modification. In low-speed applications, unfolding of the Campbell diagram is directly related to the onset of friction-induced oscillations in brakes, clutches, paper calendars and even in musical instruments like the glass harmonica (Spurr 1961; Ouyang & Mottershead 2001; Chevillot *et al.* 2008; Hervé *et al.* 2008; Kang *et al.* 2008; Kirillov 2008; Ouyang 2008; Spelsberg-Korspeter *et al.* 2009). In contrast to the supercritical instabilities, excitation of the *subcritical flutter* near the crossings, with the definite symplectic signature by the Hamiltonian perturbations only is impossible. In this case, the non-Hamiltonian dissipative and circulatory forces are required for destabilization.

In general, dissipative, $\delta\mathbf{D}$, and non-conservative positional, $\nu\mathbf{N}$, perturbations unfold MacKay's eigenvalue cones (4.1) and $(\operatorname{Re}\lambda)^2=-\operatorname{Re}c$ into the surfaces $\operatorname{Im}\lambda(\Omega,\kappa)$ and $\operatorname{Re}\lambda(\Omega,\kappa)$, described by formulas (3.4). The new eigenvalue surfaces have singularities at the *exceptional points* (Berry & Dennis 2003; Keck *et al.* 2003). The latter correspond to the double eigenvalues with the Jordan chain that is born from the parent semisimple doublet $i\omega_0$ at $\Omega=\Omega_0$. In some works, numerical methods were developed to find the coordinates of these singularities (Jones 1988; Skorokhodov 2007). Perturbation of Hamilton's diabolical points is another efficient way to locate exceptional points (Kirillov *et al.* 2005). Indeed, condition $c=0$ yields their approximate loci in the (Ω,κ)-plane

$$\Omega^{\pm}_{\mathrm{EP}}=\Omega_0\pm\frac{4\omega_s\omega_t U-\beta\omega_s\operatorname{tr}\mathbf{K}_{tt}+\alpha\omega_t\operatorname{tr}\mathbf{K}_{ss}}{4\omega_s\omega_t(t\sigma-s\varepsilon)}\sqrt{\frac{N}{D}}\quad\text{and}\quad\kappa^{\pm}_{\mathrm{EP}}=\pm\sqrt{\frac{N}{D}},\tag{5.1}$$

where

$$\left.\begin{aligned}U&=\frac{\operatorname{Re}A_2\operatorname{tr}\mathbf{K}_{st}\mathbf{J}_{\varepsilon\sigma}-\operatorname{Re}B_2\operatorname{tr}\mathbf{K}_{st}\mathbf{I}_{\varepsilon\sigma}}{\alpha\omega_s\operatorname{Im}B_1-\beta\omega_t\operatorname{Im}A_1},\\ D&=U^2+\alpha\beta\left[\left(\frac{\operatorname{tr}\mathbf{K}_{st}\mathbf{J}_{\varepsilon\sigma}}{2\sqrt{\omega_s\omega_t}}\right)^2+\left(\frac{\operatorname{tr}\mathbf{K}_{st}\mathbf{I}_{\varepsilon\sigma}}{2\sqrt{\omega_s\omega_t}}\right)^2\right],\\ N&=\left(\frac{\alpha\omega_s\operatorname{Im}B_1-\beta\omega_t\operatorname{Im}A_1}{4\omega_s\omega_t}\right)^2+\alpha\beta\left[\left(\frac{\operatorname{Re}A_2}{2\sqrt{\omega_s\omega_t}}\right)^2+\left(\frac{\operatorname{Re}B_2}{2\sqrt{\omega_s\omega_t}}\right)^2\right].\end{aligned}\right\}\tag{5.2}$$

The crossings with the definite symplectic signature ($\alpha\beta>0$) always produce a pair of exceptional points. For example, for pure non-conservative ($\delta=0$) and pure dissipative ($\nu=0$) perturbation of the doublets at $\Omega_0=0$, formulas (5.1) read

$$\left.\begin{aligned}\Omega^{\pm}_{\mathrm{EP},n}&=0,\quad \kappa^{\pm}_{\mathrm{EP},n}=\pm\frac{2\nu n_{2s-1,2s}}{\rho_1(\mathbf{K}_{ss})-\rho_2(\mathbf{K}_{ss})},\\ \Omega^{\pm}_{\mathrm{EP},d}&=\pm\delta\frac{\mu_1(\mathbf{D}_{ss})-\mu_2(\mathbf{D}_{ss})}{4s},\quad \kappa^{\pm}_{\mathrm{EP},d}=0,\end{aligned}\right\}\tag{5.3}$$

where $\rho_{1,2}(\mathbf{K}_{ss})$ are the eigenvalues of the block $\mathbf{K}_{ss}$ of the matrix $\mathbf{K}$ and $\mu_{1,2}(\mathbf{D}_{ss})$ are those of the block $\mathbf{D}_{ss}$ of $\mathbf{D}$. In the case of the mixed symplectic signature ($\alpha\beta<0$), the two exceptional points exist when $N/D>0$ and do not exist otherwise.

The strong influence of the exceptional points on the stability and their relation to Ziegler's destabilization paradox owing to small damping is well recognized (Bottema 1956; Kirillov 2005, 2006, 2007*a*,*b*; Krechetnikov & Marsden 2007; Chevillot *et al.* 2008). In numerous applications in rotor dynamics (Ono *et al.* 1991; Chen & Bogy 1992; Mottershead & Chan 1995; Yang & Hutton 1995; Tian & Hutton 1999; Xiong *et al.* 2002; Genta 2007; Lesaffre *et al.* 2007) as well as in hydrodynamics (Or 1991), crystal optics (Berry & Dennis 2003), acoustics (Shuvalov & Scott 2000) and microwave billiards (Keck *et al.* 2003), the generalized crossing scenario in the vicinity of the exceptional points has been observed (visible also in figure 1*e*,*f*) when at the same values of the parameters the imaginary parts of the eigenvalues cross, whereas the real parts do not and vice versa. In our setting, the conditions for coincidence of imaginary parts of the eigenvalues (3.4) are $\operatorname{Im} c=0$ and $\operatorname{Re} c\leq 0$ and that for coincidence of the real parts are $\operatorname{Im} c=0$ and $\operatorname{Re} c\geq 0$. Both real and imaginary parts of the eigenvalues coincide only at the two exceptional points $(\Omega^{+}_{\mathrm{EP}},\kappa^{+}_{\mathrm{EP}})$ and $(\Omega^{-}_{\mathrm{EP}},\kappa^{-}_{\mathrm{EP}})$. The segment of the line $\operatorname{Im} c=0$ connecting the exceptional points is the projection of the branch cut of a singular eigenvalue surface $\operatorname{Im}\lambda(\Omega,\kappa)$. The adjacent parts of the line correspond to the branch cuts of the singular eigenvalue surface $\operatorname{Re}\lambda(\Omega,\kappa)$. As simultaneous intersection of the different segments of the line $\operatorname{Im} c=0$ in the (Ω,κ)-plane is not possible, one observes the generalized crossing scenario (Keck *et al.* 2003; Kirillov *et al.* 2005) in the planes $(\Omega,\operatorname{Im}\lambda)$ and $(\Omega,\operatorname{Re}\lambda)$ or $(\kappa,\operatorname{Im}\lambda)$ and $(\kappa,\operatorname{Re}\lambda)$.

For example, in the case of pure non-conservative positional perturbation, the real parts of the eigenvalues developing near the doublets at $\Omega_0=0$ cross each other in the $(\Omega,\operatorname{Re}\lambda)$-plane at the points of the branch cuts $\kappa^2>(\kappa^{\pm}_{\mathrm{EP},n})^2$

$$\operatorname{Re}\lambda=\pm\frac{2\nu s n_{2s-1,2s}}{(\rho_1(\mathbf{K}_{ss})-\rho_2(\mathbf{K}_{ss}))\sqrt{\kappa^2-(\kappa^{\pm}_{\mathrm{EP},n})^2}}\Omega+O(\Omega^3),\tag{5.4}$$

whereas for $\kappa^2<(\kappa^{\pm}_{\mathrm{EP},n})^2$ they avoid crossing

$$\operatorname{Re}\lambda=\pm\frac{\rho_1(\mathbf{K}_{ss})-\rho_2(\mathbf{K}_{ss})}{4\omega_s}\sqrt{(\kappa^{\pm}_{\mathrm{EP},n})^2-\kappa^2}+O(\Omega^2).\tag{5.5}$$

At the exceptional points $\kappa=\kappa^{\pm}_{\mathrm{EP},n}$, the eigenvalue branches touch each other

$$\operatorname{Re}\lambda=\pm\frac{1}{2}\sqrt{\frac{2\nu s n_{2s-1,2s}}{\omega_s}\Omega}+O(\Omega^{3/2}).\tag{5.6}$$

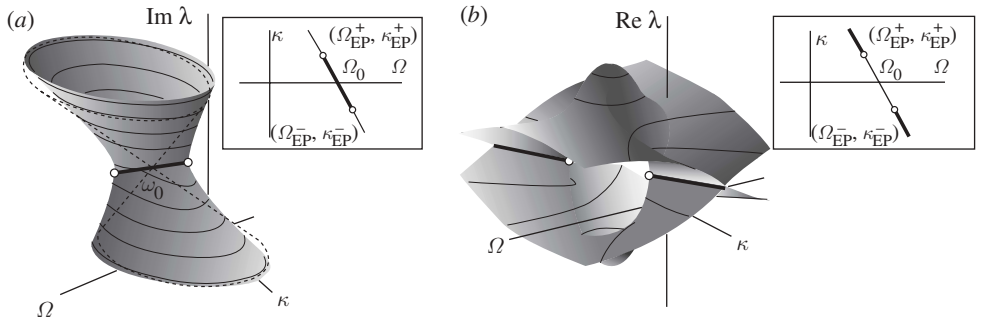

Figure 3. (*a*) The 'double coffee filter' singular surface $\mathrm{Im}\,\lambda(\Omega,\kappa)$ with the exceptional points (open circles) and branch cut (bold lines) originated from MacKay's cone (dashed lines) owing to mixed dissipative and circulatory perturbation at any crossing with the definite symplectic signature; (*b*) the corresponding 'viaduct' $\mathrm{Re}\,\lambda(\Omega,\kappa)$.

The degenerate crossing (5.6) of the real parts has been observed in the model of a rotating circular string (Yang & Hutton 1995; Kirillov 2008).

Pure dissipative perturbation of the doublets at $\Omega_0=0$ yields crossings of the real parts at the branch cuts $\Omega^2>(\Omega^{\pm}_{\mathrm{EP},d})^2$ in the $(\mathrm{Re}\,\lambda,\kappa)$-plane and veering of the imaginary parts

$$\left.\begin{aligned}\mathrm{Im}\,\lambda&=\omega_s\pm s\sqrt{\Omega^2-(\Omega^{\pm}_{\mathrm{EP},d})^2}+O(\kappa),\\ \mathrm{Re}\,\lambda&=-\frac{\delta\,\mathrm{tr}\,\mathbf{D}_{ss}}{4}\pm\frac{\gamma}{16s\omega_s\sqrt{\Omega^2-(\Omega^{\pm}_{\mathrm{EP},d})^2}}\delta\kappa+O(\kappa^3),\end{aligned}\right\}\tag{5.7}$$

where $\gamma=2\,\mathrm{tr}\,\mathbf{K}_{ss}\mathbf{D}_{ss}-\mathrm{tr}\,\mathbf{K}_{ss}\,\mathrm{tr}\,\mathbf{D}_{ss}$. At the branch cut $\Omega^2<(\Omega^{\pm}_{\mathrm{EP},d})^2$, the imaginary parts cross and the real parts avoid crossing

$$\left.\begin{aligned}\mathrm{Im}\,\lambda&=\omega_s+\frac{\mathrm{tr}\,\mathbf{K}_{ss}}{4\omega_s}\kappa\pm\frac{\gamma}{16s\omega_s\sqrt{(\Omega^{\pm}_{\mathrm{EP},d})^2-\Omega^2}}\delta\kappa+O(\kappa^2),\\ \mathrm{Re}\,\lambda&=-\frac{\delta\,\mathrm{tr}\,\mathbf{D}_{ss}}{4}\pm s\sqrt{(\Omega^{\pm}_{\mathrm{EP},d})^2-\Omega^2}+O(\kappa^2).\end{aligned}\right\}\tag{5.8}$$

At $\Omega=\Omega^{\pm}_{\mathrm{EP},d}$, the crossings of both real and imaginary parts are degenerate

$$\left.\begin{aligned}\mathrm{Re}\,\lambda&=-\frac{\delta\,\mathrm{tr}\,\mathbf{D}_{ss}}{4}\pm\frac{1}{4}\sqrt{-\delta\kappa\frac{\gamma}{\omega_s}}+O(\kappa^{3/2}),\\ \mathrm{Im}\,\lambda&=\omega_s\pm\frac{1}{4}\sqrt{-\delta\kappa\frac{\gamma}{\omega_s}}+\frac{\mathrm{tr}\,\mathbf{K}_{ss}}{4\omega_s}\kappa+O(\kappa^{3/2}).\end{aligned}\right\}\tag{5.9}$$

The evolving eigenvalue branches reconstruct the eigenvalue surfaces shown in figure 3. In the one-parameter slices of the surfaces, the transformation of the eigenvalue branches from the crossing to the avoided crossing owing to the variation of the parameters Ω and κ occurs after the passage through the exceptional points, where the branches touch each other and the eigenvalue

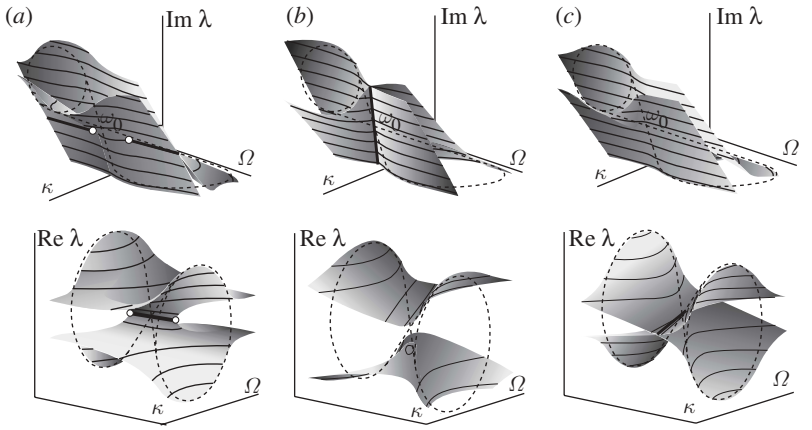

Figure 4. Mixed symplectic signature ($\alpha\beta < 0$): (a) The viaduct $\mathrm{Im}\,\lambda(\Omega,\kappa)$ and the double coffee filter $\mathrm{Re}\,\lambda(\Omega,\kappa)$ for $D < 0$ and $N < 0$; (b) the surfaces $\mathrm{Im}\,\lambda(\Omega,\kappa)$ crossed along the branch cut (bold line) and the separated surfaces $\mathrm{Re}\,\lambda(\Omega,\kappa)$ for $D < 0$, $N > 0$; (c) separated surfaces of imaginary parts and crossed surfaces of real parts for $D > 0$, $N < 0$.

surfaces have Whitney's umbrella singularities. The surface of the imaginary parts shown in figure 3*a* is formed by the two Whitney's umbrellas with the handles (branch cuts) glued when they are oriented towards each other. This singular surface is known in the physical literature on wave propagation in anisotropic media as the *double coffee filter* (Berry & Dennis 2003; Keck *et al.* 2003). The *viaduct* singular surface of the real parts results from the gluing of the roofs of two Whitney's umbrellas when their handles are oriented outwards (figure 3*b*). The double coffee filter singularity is a result of the deformation of MacKay's eigenvalue cone (shown by the dashed lines in figure 3*a*) by dissipative and non-conservative positional perturbations. The perturbations foliate the plane $\mathrm{Re}\,\lambda = 0$ into the viaduct, which has self-intersections along two branch cuts and an ellipse-shaped arch between the two exceptional points, figure 3*b*. Both types of singular surfaces appear when non-Hermitian perturbation of Hermitian matrices is considered (Kahan 1975; Kirillov *et al.* 2005).

Therefore, in a weakly non-Hamiltonian system (2.1), the fundamental qualitative effect of the splitting of the doublets with the definite symplectic (Krein) signature is the origination of the double coffee filter of the imaginary parts and the viaduct of the real parts. Structural modification of the matrices of dissipative and non-conservative positional forces generically does not change the type of the surfaces, preserving the exceptional points and the branch cuts.

6. Unfolding MacKay's cones with mixed signature

The definite symplectic signature ($\alpha\beta > 0$) implies $D > 0$ and $N > 0$ and thus uniquely determines the type of the singular surface for the real and imaginary parts of the perturbed eigenvalues. The case of the mixed symplectic signature ($\alpha\beta < 0$) possesses several scenarios for the unfolding of MacKay's cones by the non-Hamiltonian perturbation because D and N can have different signs.

When $D>0$ and $N>0$, the imaginary parts of the eigenvalues form the double coffee filter singular surface whereas the real parts originate the viaduct (figure 3). For negative D and negative N, the type of the surfaces is interchanged: the imaginary parts form the viaduct and the real parts originate the double coffee filter (figure 4*a*).

Exceptional points are not created for negative values of N/D. In this case, the eigenvalue surfaces either intersect each other along the branch cut, which projects into the line $\mathrm{Im}\, c=0$ in the (Ω,κ)-plane, or do not cross at all. When $N>0$, the surfaces of the imaginary parts $\mathrm{Im}\,\lambda(\Omega,\kappa)$ cross and the surfaces $\mathrm{Re}\,\lambda(\Omega,\kappa)$ avoid crossing (figure 4*b*). For $N<0$, the surfaces of the imaginary parts are separated and those of the real parts cross (figure 4*c*).

7. Example 1: a rotating shaft

The simplest mechanical systems described by equations (2.1) and (2.2) are some models of rotating shafts (Kimball 1924; Shieh & Masur 1968; Nagata & Namachchivaya 1998; Genta 2007). In Shieh & Masur (1968), the shaft is modelled as the mass m, which is attached by two springs with the stiffness coefficients k_1 and $k_2=k_1+\kappa$ and two dampers with the coefficients μ_1 and μ_2 to a coordinate system rotating at a constant angular velocity Ω (figure 5*a*). A non-conservative positional force βr acts on the mass. With u and v representing the displacements in the direction of the two rotating coordinate axes, respectively, the system is governed by the equations (Shieh & Masur 1968)

$$\left.\begin{aligned} m\ddot{u}+\mu_1\dot{u}-2m\Omega\dot{v}+(k_1-m\Omega^2)u+\beta v=0,\\ m\ddot{v}+\mu_2\dot{v}+2m\Omega\dot{u}+(k_2-m\Omega^2)v-\beta u=0. \end{aligned}\right\} \tag{7.1}$$

In figure 5*b*, we show a numerically found surface of frequencies for the shaft with $m=1$ and $k_1=4$ in the absence of damping and non-conservative forces. The surface has four conical singularities corresponding to the doublets $\pm 2i$ at $\Omega=0$ and to the double-zero eigenvalues at the critical speeds $\Omega=\pm 2$. The cones in the subcritical speed range are near-vertically oriented while those at the critical speeds are near horizontal. Consequently, for small stiffness detuning κ, the system is stable in the subcritical speed range and unstable by divergence in the vicinity of the critical speeds, where the bubbles of instability in the decay rate plots originate.

Addition of the non-conservative forces with $\beta=0.2$ and damping with $\mu_1=0.1$ and $\mu_2=0.2$ yields deformation of the conical surfaces with apexes at $\Omega=0$ into the double coffee filters. The real parts form the viaduct singular surfaces shown in figure 5*c*,*d*. In the absence of damping ($\mu_{1,2}=0$), the gyroscopic system with the potential and non-conservative positional forces cannot be asymptotically stable in accordance with the theorem of Lakhadanov (1975). It is unstable almost everywhere in the space of parameters and can be only marginally stable on the set of measure zero in it. This is seen in figure 5*c*, which shows that the shaft is marginally stable at the points of the branch cuts, that form the set of measure zero and unstable at all other points of the parameter plane.

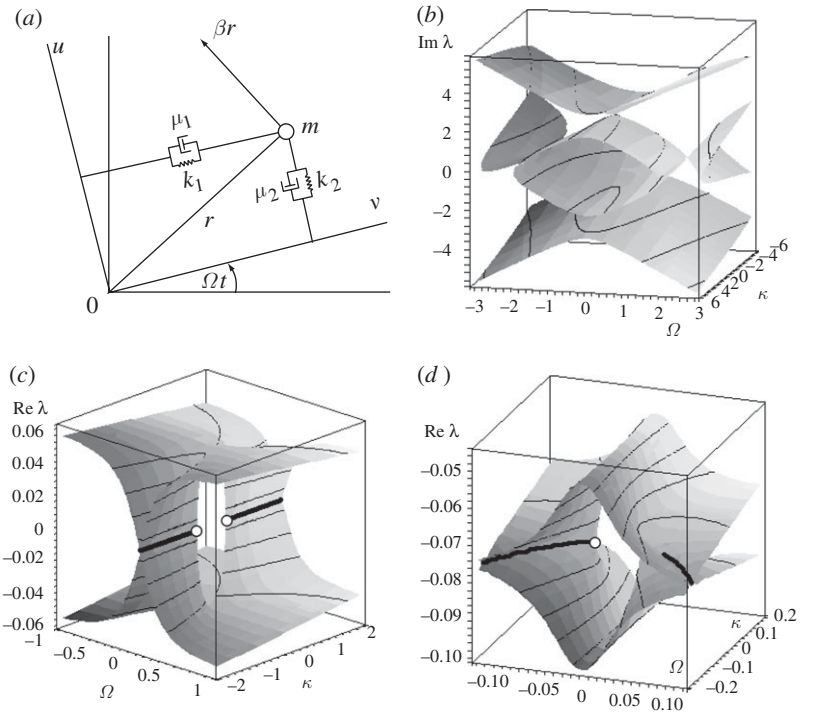

Figure 5. (*a*) A model of the rotating shaft; (*b*) four MacKay's cones owing to stiffness modification ($\mu_1 = 0$, $\mu_2 = 0$, $\beta = 0$); (*c*) the viaduct singular surface created by the circulatory force only ($\beta = 0.2$); and (*d*) by the damping only ($\mu_1 = 0.1$, $\mu_2 = 0.2$).

8. Example 2: a rotating circular string

Consider a circular string of displacement $W(\varphi, \tau)$, radius r and mass per unit length ρ that rotates with the speed γ and passes at $\varphi = 0$ through a massless eyelet, generating a constant frictional follower force F on the string (Yang & Hutton 1995). The circumferential tension P in the string is constant; the stiffness of the spring supporting the eyelet is K and the damping coefficient of the viscous damper is D; the velocity of the string in the φ direction has a constant value γr.

With the non-dimensional variables and parameters

$$t = \frac{\tau}{r}\sqrt{\frac{P}{\rho}}, \quad w = \frac{W}{r}, \quad \Omega = \gamma r\sqrt{\frac{\rho}{P}}, \quad k = \frac{Kr}{P}, \quad \mu = \frac{F}{P} \quad \text{and} \quad d = \frac{D}{\sqrt{\rho P}}, \tag{8.1}$$

the substitution of $w(\varphi, t) = u(\varphi)\exp(\lambda t)$ into the governing equation and boundary conditions yields the boundary eigenvalue problem (Yang & Hutton 1995)

$$Lu = \lambda^2 u + 2\Omega\lambda u' - (1 - \Omega^2)u'' = 0, \tag{8.2}$$

$$u(0) - u(2\pi) = 0 \quad \text{and} \quad u'(0) - u'(2\pi) = \frac{\lambda d + k}{1 - \Omega^2}u(0) + \frac{\mu}{1 - \Omega^2}u'(0), \tag{8.3}$$

where $' = \partial_\varphi$. The boundary eigenvalue problem (8.2) and (8.3) depends on the speed of rotation (Ω), and damping (d), stiffness (k) and friction (μ) coefficients.

We note that the artificialness of the term, corresponding to the non-conservative positional forces, in the second of the boundary conditions (8.3), was discussed in the literature (Yang & Hutton 1995; Kirillov 2008). We keep it, however, to show how the degeneracy of this operator is seen in the eigenvalue surfaces.

For $d=0$, $k=0$ and $\mu=0$, the eigenvalue problem (8.2) and (8.3) has the eigenvalues $\lambda_n^\varepsilon = in(1+\varepsilon\Omega)$, $\lambda_m^\delta = im(1+\delta\Omega)$, where $\varepsilon,\delta=\pm1$ and $n,m\in\mathbb{Z}-\{0\}$. In the $(\Omega,\operatorname{Im}\lambda)$-plane, the branches intersect each other at the node (Ω_0,ω_0) with

$$\Omega_0 = \frac{n-m}{m\delta-n\varepsilon} \quad \text{and} \quad \omega_0 = \frac{nm(\delta-\varepsilon)}{m\delta-n\varepsilon}, \tag{8.4}$$

where the double eigenvalue $\lambda_0 = i\omega_0$ has two linearly independent eigenfunctions

$$u_n^\varepsilon = \cos(n\varphi) - \varepsilon i\sin(n\varphi) \quad \text{and} \quad u_m^\delta = \cos(m\varphi) - \delta i\sin(m\varphi). \tag{8.5}$$

Intersections of the branch with $n=1$ and $\varepsilon=1$ and the branches with $m>0$ and $\delta<0$ in the subcritical range ($|\Omega|<1$) are marked in figure 6*a* by red dots.

Taking into account that $\delta=-\varepsilon$ at all the crossings, excluding ($\Omega_0=\pm1$, $\omega_0=0$) where $\delta=\varepsilon$, we find approximations to the real and imaginary parts of the perturbed non-zero double eigenvalues (Kirillov 2008)

$$\left.\begin{aligned}
\operatorname{Re}\lambda &= -d\frac{n+m}{8\pi nm}\omega_0 \pm \sqrt{\frac{|c|-\operatorname{Re}c}{2}},\\
\operatorname{Im}\lambda &= \omega_0 + \varepsilon\frac{n-m}{2}\Delta\Omega + \frac{n+m}{8\pi nm}k \pm \sqrt{\frac{|c|+\operatorname{Re}c}{2}},
\end{aligned}\right\} \tag{8.6}$$

where $\Delta\Omega = \Omega - \Omega_0$, and for the complex coefficient c, we have

$$\left.\begin{aligned}
\operatorname{Im}c &= k\frac{2d\omega_0 - \varepsilon\mu(n-m)}{16\pi^2 nm} - 2\left(\varepsilon\frac{n+m}{2}\Delta\Omega + \frac{m-n}{8\pi nm}k\right)\left(\frac{\varepsilon}{4\pi}\mu - d\frac{m-n}{8\pi nm}\omega_0\right),\\
\operatorname{Re}c &= \left(\frac{\varepsilon n-\delta m}{2}\Delta\Omega + \frac{m-n}{8\pi nm}k\right)^2 + \frac{k^2}{16\pi^2 nm} - \frac{[d(m+n)\omega_0]^2}{64\pi^2 n^2 m^2}.
\end{aligned}\right\} \tag{8.7}$$

Setting $\operatorname{Re}c=0$ and $\operatorname{Im}c=0$, we find the coordinates of the projections of the exceptional points of the surfaces $\operatorname{Re}\lambda(\Omega,k)$ and $\operatorname{Im}\lambda(\Omega,k)$ onto the (Ω,k)-plane

$$\left.\begin{aligned}
\Omega_{\mathrm{EP}} &= \Omega_0 \pm \frac{\varepsilon}{8\pi nm}\frac{(m+n)d^2\omega_0^2}{\sqrt{nm(\mu^2 nm + d^2\omega_0^2)}},\\
\kappa_{\mathrm{EP}} &= \pm\frac{d\omega_0(2\varepsilon\mu nm - d(m-n)\omega_0)}{2\sqrt{nm(\mu^2 nm + d^2\omega_0^2)}}.
\end{aligned}\right\} \tag{8.8}$$

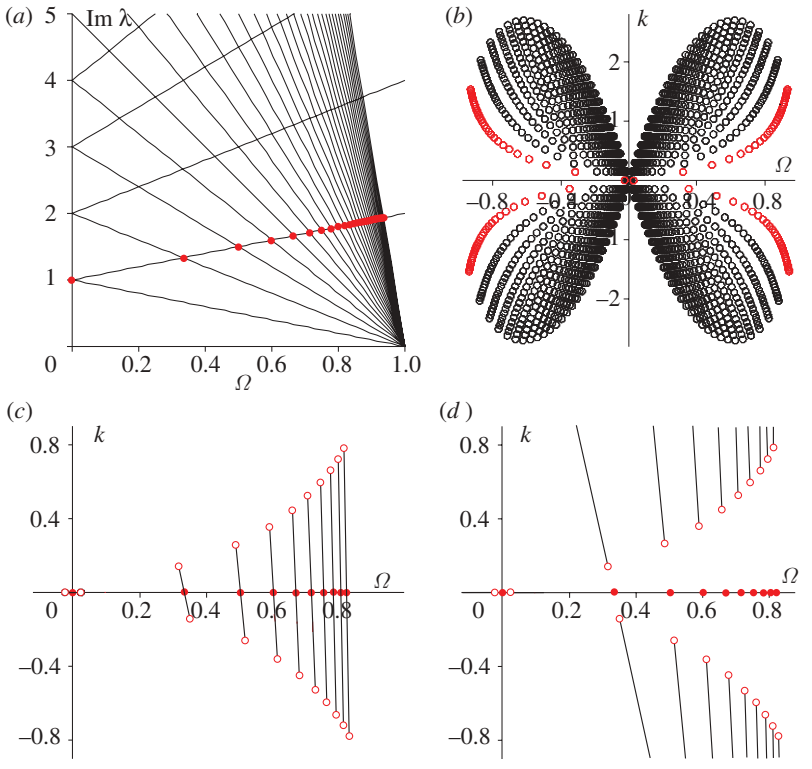

Figure 6. (*a*) The Campbell diagram of the unperturbed rotating string with red dots marking the nodes with $n=1$; (*b*) a butterfly distribution (8.8) of the exceptional points (open circles) in the subcritical speed range in the (Ω,k)-plane when $\mu=0$ and $d=0.3$ (red open circles correspond to $n=1$); (*c*) projections of the branch cuts (8.9) of the coffee filters $\operatorname{Im}\lambda(\Omega,k)$ and the exceptional points for $n=1$; (*d*) projections of the branch cuts (8.9) of the viaducts $\operatorname{Re}\lambda(\Omega,k)$ and the exceptional points for $n=1$.

As in formulas (5.1), the existence of the exceptional points (8.8) depends on the symplectic (Krein) signature of the intersecting branches, i.e. on the sign of nm, where $n,m\in\mathbb{Z}-\{0\}$. In the case of the rotating string, all the crossings in the subcritical speed range ($|\Omega|<1$) have definite Krein signature ($nm>0$). For those in the supercritical speed range ($|\Omega|>1$), it is mixed with $nm<0$. In the (Ω,κ)-plane, the exceptional points are situated on the line $\operatorname{Im} c=0$

$$k=2\pi\varepsilon(n+m)\frac{2\varepsilon nm\mu-d\omega_0(m-n)}{d\omega_0(m^2+n^2)}\Delta\Omega. \tag{8.9}$$

In figure 6*b*, we show the exceptional points (8.8) of the string passing through the eyelet with the damping coefficient $d=0.3$. The red open circles correspond to the exceptional points born after the splitting of the diabolical crossings with $n=1$ and $\varepsilon=1$, which are shown in figure 6*a* by red dots. The exceptional points in the (Ω,κ)-plane are distributed over a butterfly-shaped area, which preserves its form independently of the number of points involved. In comparison with the numerical methods of Jones (1988) and Skorokhodov (2007), our perturbation

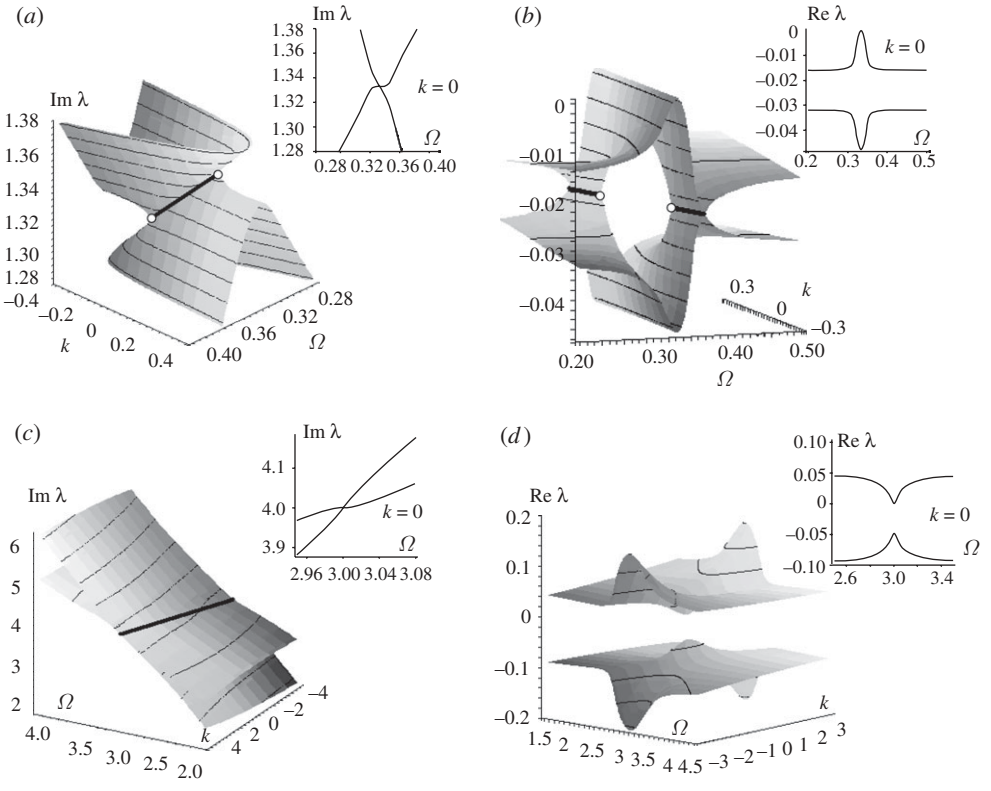

Figure 7. For $d = 0.3$ and $\mu = 0$: (a) the double coffee filter singular surface $\mathrm{Im}\,\lambda(\Omega, k)$ in the vicinity of the crossing $(n = 1, m = 2)$; (b) the viaduct surface $\mathrm{Re}\,\lambda(\Omega, k)$ corresponding to the crossing $(n = 1, m = 2)$; (c) intersecting surfaces $\mathrm{Im}\,\lambda(\Omega, k)$ in the vicinity of the crossing $(n = 1, m = -2)$; and (d) the corresponding non-intersecting surfaces $\mathrm{Re}\,\lambda(\Omega, k)$.

approach gives efficient explicit and interpretable expressions for the distribution of the exceptional points, for the branch cuts and for the very eigenvalue surfaces.

In figure 6*c*, we plot the exceptional points originated after the splitting of the diabolical points with $n = 1$ and $\varepsilon = 1$ together with the projections of the branch cuts (8.9) of the double coffee filters $\mathrm{Im}\,\lambda(\Omega, k)$, which are shown by bold lines. The corresponding projections of the branch cuts (8.9) of the viaducts $\mathrm{Re}\,\lambda(\Omega, k)$ are presented in figure 6*d*. Only exceptional points originated after the perturbation of the doublets with $\Omega_0 = 0$ are situated on the Ω-axis. This explains why damping creates a perfect bubble of instability for the doublets with $m = n$ and imperfect ones for the diabolical points with $m \neq n$ (Yang & Hutton 1995; Kirillov 2008). Approximations (8.6) to the eigenvalue surfaces of a string with $\mu = 0$ and $d = 0.3$ are presented in figure 7 for different values of n, m, ε and δ. The smaller inclusions in figure 7 show the cross sections of the surfaces by the plane $k = 0$ for the convenience of comparing with the numerical data of Yang & Hutton (1995). The results shown in figure 7 are in qualitative agreement with the developed theory for equations (2.1) and (2.2) and perfectly agree with the numerical modelling.

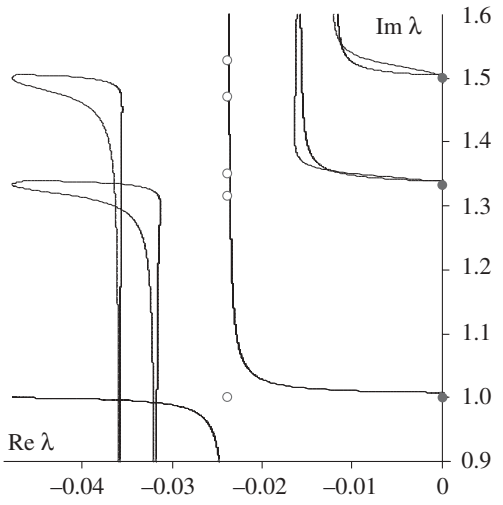

Figure 8. Exceptional points (open circles) with the parent diabolical points with $n=1$, $\varepsilon=1$ in the complex plane when $d=0.3$ and the trajectories $\lambda(\Omega)$ for $k=0.05$.

In figure 8, we show in the complex plane the parent diabolical points (grey dots) and the corresponding exceptional points (open circles) whose locations are

$$\operatorname{Re}\lambda_{\mathrm{EP}}=-\frac{d}{4\pi}\quad\text{and}\quad\operatorname{Im}\lambda_{\mathrm{EP}}=\frac{2nm}{n+m}\pm\frac{d}{4\pi}\frac{n-m}{\sqrt{nm}}. \tag{8.10}$$

In the engineering literature, it was observed that the exceptional points (*strong modal resonances* Dobson *et al.* 2001) are precursors to flutter instability because of their strong influence on the movement of eigenvalues in the complex plane. Figure 8 demonstrates the approximation of the 'dynamics' of eigenvalues in the vicinity of the exceptional points, calculated by formulas (8.6), which is in a good qualitative agreement with the known numerical results (Sinou *et al.* 2006).

Finally, we notice that pure non-conservative positional perturbation ($d=0$) causes degeneration of the eigenvalue surfaces. Indeed, the line (8.9) reduces to $\Omega=\Omega_0$ and the two exceptional points merge into one at $\Omega_{\mathrm{EP}}=\Omega_0$ and $\kappa_{\mathrm{EP}}=0$. As a consequence, the central arch of the viaduct and the branch cut of the double coffee filter shrink to a single point. At this exceptional point, the angle of crossing of the surfaces is zero in agreement with Yang & Hutton (1995) and Kirillov (2008). This degeneration visualizes the artificialness of the term related to the friction force in equation (8.7) that was already pointed out in the literature by physical arguments.

9. Conclusion

We found that in a weakly anisotropic rotor system (2.1), the branches of the Campbell diagram and the decay rate plots in the subcritical speed range are the cross sections of the two companion singular eigenvalue surfaces. The double

coffee filter and the viaduct are the imaginary and the real part of the unfolding of any double pure imaginary semisimple eigenvalue at the crossing of the Campbell diagram with the definite symplectic (Krein) signature. Generically, the structure of the perturbing matrices determines only the details of the geometry of the surfaces, such as the coordinates of the exceptional points and the spatial orientation of the branch cuts. It does not yield qualitative changes irrespective of whether dissipative and circulatory perturbations are applied separately or in a mixture. The two eigenvalue surfaces found unite seemingly different problems on friction-induced instabilities in rotating elastic continua because their existence does not depend on the specific model of the rotor–stator interaction and is dictated by the symplectic signature of the eigenvalues of the isotropic rotor and by the non-conservative nature of the forces originated at the frictional contact. The double coffee filter singularity and its viaduct companion are true symbols of instabilities causing the wine glass to sing and the brake to squeal that connect these phenomena of the wave propagation in rotating continua with the physics of non-Hermitian singularities associated with the wave propagation in stationary anisotropic chiral media (Berry 2004).

The study has been supported by the research grant DFG HA 1060/43-1.

References

Berry, M. V. 2004 Physics of non-Hermitian degeneracies. *Czech. J. Phys.* **54**, 1039–1047. (doi:10.1023/B:CJOP.0000044002.05657.04)

Berry, M. V. & Dennis, M. R. 2003 The optical singularities of birefringent dichroic chiral crystals. *Proc. R. Soc. Lond. A* **459**, 1261–1292. (doi:10.1098/rspa.2003.1155)

Berry, M. V. & Jeffrey, M. R. 2007 *Chapter 2* Conical diffraction: Hamilton's diabolical point at the heart of crystal optics. *Prog. Opt.* **50**, 13–50. (doi:10.1016/S0079-6638(07)50002-8)

Bottema, O. 1956 The Routh-Hurwitz condition for the biquadratic equation. *Indag. Math.* **18**, 403–406.

Bryan, G. 1890 On the beats in the vibrations of a revolving cylinder or bell. *Proc. Camb. Phil. Soc.* **7**, 101–111.

Campbell, W. 1924 The protection of steam-turbine disk wheels from axial vibration. *Trans. ASME* **46**, 31–160.

Canchi, S. V. & Parker, R. G. 2006 Parametric instability of a circular ring subjected to moving springs. *J. Sound Vib.* **293**, 360–379. (doi:10.1016/j.jsv.2005.10.007)

Chen, J.-S. & Bogy, D. B. 1992 Mathematical structure of modal interactions in a spinning disk-stationary load system. *Trans. ASME J. Appl. Mech.* **59**, 390–397. (doi:10.1115/1.2899532)

Chevillot, F., Sinou, J.-J., Mazet, G.-B., Hardouin, N. & Jézéquel, L. 2008 The destabilization paradox applied to friction-induced vibrations in an aircraft braking system. *Arch. Appl. Mech.* **78**, 949–963. (doi:10.1007/S00419-008-0208-7)

Dellnitz, M., Melbourne, I. & Marsden, J. E. 1992 Generic bifurcation of Hamiltonian vector fields with symmetry. *Nonlinearity* **5**, 979–996. (doi:10.1088/0951-7715/5/4/008)

Dobson, I., Zhang, J., Greene, S., Engdahl, H. & Sauer, P. W. 2001 Is strong modal resonance a precursor to power system oscillations? *IEEE Trans. Circ. Syst. I* **48**, 340–349.

Genta, G. 2007 *Dynamics of rotating systems*. New York, NY: Springer.

Günther, U. & Kirillov, O. N. 2006 A Krein space related perturbation theory for MHD α^2-dynamos and resonant unfolding of diabolical points. *J. Phys. A Math. Gen.* **39**, 10 057–10 076. (doi:10.1088/0305-4470/39/32/S08)

Hamilton, W. R. 1833 On a general method of expressing the paths of light, and of the planets, by the coefficients of a characteristic function. *Dublin Univ. Rev. Q. Mag.* **1**, 795–826.

Hervé, B., Sinou, J.-J., Mahé, H. & Jézéquel, L. 2008 Analysis of squeal noise and mode coupling instabilities including damping and gyroscopic effects. *Eur. J. Mech. A.* **27**, 141–160. (doi:10.1016/j.euromechsol.2007.05.004)

Hirota, M. & Fukumoto, Y. 2008 Energy of hydrodynamic and magnetohydrodynamic waves with point and continuous spectra. *J. Math. Phys.* **49**, 083 101. (doi: 10.1063/1.2969275)

Jones, C. A. 1988 Multiple eigenvalues and mode classification in plane Poiseuille flow. *Quart. J. Mech. Appl. Math.* **41** 363–382. (doi:10.1093/qjmam/41.3.363)

Kahan, W. 1975 Spectra of nearly Hermitian matrices *Proc. Amer. Math. Soc.* **48**, 11–17. (doi: 10.2307/2040683)

Kang, J., Krousgrill, C. M. & Sadeghi, F. 2008 Dynamic instability of a thin circular plate with friction interface and its application to disc brake squeal. *J. Sound Vib.* **316**, 164–179. (doi: 10.1016/j.jsv.2008.02.041)

Keck, F., Korsch, H. J. & Mossmann, S. 2003 Unfolding a diabolic point: a generalized crossing scenario. *J. Phys. A Math. Gen.* **36**, 2125–2137. (doi: 10.1088/0305-4470/36/8/310)

Kimball, A. L. 1924 Internal friction theory of shaft whirling. *Gen. Electric Rev.* **27**, 244–251.

Kirillov, O. N. 2005 A theory of the destabilization paradox in non-conservative systems. *Acta Mech.* **174**, 145–166. (doi:10.1007/S00707-004-0194-y)

Kirillov, O. N. 2006 Gyroscopic stabilization of non-conservative systems. *Phys. Lett. A* **359**, 204–210. (doi:10.1016/j.physleta.2006.06.040)

Kirillov, O. N. 2007*a* Destabilization paradox due to breaking the Hamiltonian and reversible symmetry. *Int. J. Nonlin. Mech.* **42**, 71–87. (doi:10.1016/j.ijnonlinmec.2006.09.003)

Kirillov, O. N. 2007*b* Gyroscopic stabilization in the presence of nonconservative forces. *Dokl. Math.* **76**, 780–785. (doi:10.1134/S1064562407050353)

Kirillov, O. N. 2008 Subcritical flutter in the acoustics of friction. *Proc. R. Soc. A* **464**, 2321–2339. (doi:10.1098/rspa.2008.0021)

Kirillov, O. N. 2009*a* Unfolding the conical zones of the dissipation-induced subcritical flutter for the rotationally symmetrical gyroscopic systems. *Phys. Lett. A* **373**, 940–945. (doi:10.1016/j.Physleta.2009.01.013)

Kirillov, O. N. 2009*b* Perspectives and obstacles for optimization of brake pads with respect to stability criteria. *Int. J. Veh. Des.* **51**, 143–167.

Kirillov, O. N., Mailybaev, A. A. & Seyranian, A. P. 2005 Unfolding of eigenvalue surfaces near a diabolic point due to a complex perturbation. *J. Phys. A Math. Gen.* **38**, 5531–5546. (doi:1088/0305-4470/38/24/007)

Kirillov, O. N., Günther, U. & Stefani, F. 2009 Determining role of Krein signature for three-dimensional Arnold tongues of oscillatory dynamos. *Phys. Rev. E.* **79** 016 205. (doi:10.1103/PhysRevE.79.016205)

Krechetnikov, R. & Marsden, J. E. 2007 Dissipation-induced instabilities in finite dimensions. *Rev. Mod. Phys.* **79**, 519–553. (doi:10.1103/RevModPhys.79.519)

Krein, M. G. 1983 *Topics in differential and integral equations and operator theory.* Basel, Switzerland: Birkhäuser.

Lakhadanov, V. M. 1975 On stabilization of potential systems. *Prikl. Mat. Mekh.* **39**, 53–58.

Lesaffre, N., Sinou, J.-J. & Thouverez, F. 2007 Contact analysis of a flexible bladed-rotor. *Eur. J. Mech. - A/Solids* **26**, 541–557. (doi:10.1016/j.euromechsol.2006.11.002)

MacKay, R. S. 1986 Stability of equilibria of Hamiltonian systems. In *Nonlinear phenomena and chaos* (ed. S. Sarkar), pp. 254–270. Bristol, UK: Adam Hilger.

MacKay, R. S. & Saffman, P. G. 1986 Stability of water waves. *Proc. R. Soc. Lond. A* **406**, 115–125. (doi:10.1098/rspa.1986.0068)

MacKay, R. S. & Sepulchre, J.-A. 1998 Stability of discrete breathers. *Phys. D* **119**, 148–162. (doi:10.1016/S0167-2789(98)00073-6)

Mondragon, A. & Hernandez, E. 1993 Degeneracy and crossing of resonance energy surfaces. *J. Phys. A Math. Gen.* **26**, 5595–5611. (doi:10.1088/0305-4470/26/20/039)

Mottershead, J. E. & Chan, S. N. 1995 Flutter instability of circular discs with frictional follower loads. *Trans. ASME J. Vib. Acoust.* **177**, 161–163. (doi:10.1115/1.2873860)

Nagata, W. & Namachchivaya, N. S. 1998 Bifurcations in gyroscopic systems with an application to rotating shafts. *Proc. R. Soc. Lond. A* **454**, 543–585. (doi:10.1098/rspa.1998.0174)

Ono, K., Chen, J.-S. & Bogy, D. B. 1991 Stability analysis for the head-disk interface in a flexible disk drive. *Trans. ASME J. Appl. Mech.* **58**, 1005–1014. (doi:10.1115/1.2897675)

Or, A. C. 1991 On the behaviour of a pair of complex eigenmodes near a crossing. *Quart. J. Mech. Appl. Math.* **44**, 559–569. (doi:10.1093/qjmam/44.4.559)

Ouyang, H. 2008 Prediction and assignment of latent roots of damped asymmetric systems by structural modifications. *Mech. Syst. Sign. Proc.* **23**, 1920–1930. (doi:10.1016/j.ymssp.2008.08.001).

Ouyang, H. & Mottershead, J. E. 2001 Unstable travelling waves in the friction-induced vibration of discs. *J. Sound Vib.* **248**, 768–779. (doi:10.1006/jsvi.2001.3720)

Shieh, R. C. & Masur, E. F. 1968 Some general principles of dynamic instability of solid bodies. *Z. Angew. Math. Phys.* **19**, 927–941. (doi:10.1007/BF01602273)

Shuvalov, A. L. & Scott, N. H. 2000 On singular features of acoustic wave propagation in weakly anisotropic thermoviscoelasticity. *Acta Mech.* **140**, 1–15. (doi:10.1007/BF01175976)

Sinou, J.-J., Thouverez, F. & Jézéquel, L. 2006 Stability analysis and non-linear behaviour of structural systems using the complex non-linear modal analysis. *Comput. Struct.* **84**, 1891–1905. (doi:10.1016/j.compstruc.2006.08.020)

Skorokhodov, S. L. 2007 Branch points of eigenvalues of the Orr–Sommerfeld operator. *Dokl. Math.* **76**, 744–749. (doi:10.1134/S1064562407050274)

Southwell, R. 1921 On the free transverse vibrations of a uniform circular disc clamped at its centre; and on the effect of rotation. *Proc. R. Soc. Lond. A* **101**, 133–153. (doi:10.1098/rspa.1922.0032)

Spelsberg-Korspeter, G., Hochlenert, D., Kirillov, O. N. & Hagedorn, P. 2009 In- and out-of-plane vibrations of a rotating plate with frictional contact: investigations on squeal phenomena. *Trans. ASME J. Appl. Mech.* **76**, 041 006. (doi:10.1115/1.3112734)

Spurr, R. T. 1961 The ringing of wine glasses. *Wear* **4**, 150–153. (doi:10.1016/0043-1648(61)90317-9)

Srinivasan, A. V. & Lauterbach, G. F. 1971 Traveling waves in rotating cylindrical shells. *Trans. ASME. J. Eng. Ind.* **93**, 1229–1231.

Stepanyants, Yu. A. & Fabrikant, A. L. 1989 Propagation of waves in hydrodynamic shear flows. *Sov. Phys. Usp.* **32**, 783–805. (doi:10.1070/PU1989v032n09ABEH002757)

Teller, E. 1937 The crossing of potential surfaces. *J. Phys. Chem.* **41**, 109–116. (doi:10.1021/j150379a010)

Tian, J. & Hutton, S. G. 1999 Self-excited vibration in flexible rotating discs subjected to various transverse interactive forces: a general approach. *Trans. ASME. J. Appl. Mech.* **66**, 800–805. (doi:10.1115/1.2791758)

Von Neumann, J. & Wigner, E. P. 1929 Über das Verhalten von Eigenwerten bei adiabatischen Prozessen. *Z. Phys.* **30**, 467–470.

Williamson, J. 1936 On the algebraic problem concerning the normal forms of linear dynamical systems. *Am. J. Math.* **58**, 141–163. (doi:10.2307/2371062)

Xiong, L. G., Chen, H. & Yi, J. M. 2002 Instability mechanism of a rotating disc subjected to various transverse interactive forces. *J. Mater. Process. Technol.* **129**, 534–538. (doi:10.1016/S0924-0136(02)00629-5)

Yang, L. & Hutton, S. G. 1995 Interactions between an idealized rotating string and stationary constraints. *J. Sound Vib.* **185**, 139–154. (doi:10.1006/jsvi.1994.0368)

Young, T. H. & Lin, C. Y. 2006 Stability of a spinning disk under a stationary oscillating unit. *J. Sound Vib.* **298**, 307–318. (doi:10.1016/j.jsv.2006.05.024)